

A Novel Passive Occupational Shoulder Exoskeleton With Adjustable Peak Assistive Torque Angle For Overhead Tasks

Jin Tian, *Graduate Student Member, IEEE*, Haiqi Zhu, Changjia Lu, Chifu Yang, Yingjie Liu, Baichun Wei, and Chunzhi Yi, *Member, IEEE*

Abstract—Objective: Overhead tasks are a primary inducement to work-related musculoskeletal disorders. Aiming to reduce shoulder physical loads, passive shoulder exoskeletons are increasingly prevalent in the industry due to their lightweight, affordability, and effectiveness. However, they can only handle specific tasks and struggle to balance compactness with a sufficient range of motion effectively. **Method:** We proposed a novel passive occupational shoulder exoskeleton designed to handle various overhead tasks at different arm elevation angles, ensuring sufficient ROM while maintaining compactness. By formulating kinematic models and simulations, an ergonomic shoulder structure was developed. Then, we presented a torque generator equipped with an adjustable peak assistive torque angle to switch between low and high assistance phases through a passive clutch mechanism. Ten healthy participants were recruited to validate its functionality by performing the screwing task. **Results:** Measured range of motion results demonstrated that the exoskeleton can ensure a sufficient ROM in both sagittal (164°) and horizontal (158°) flexion/extension movements. The experimental results of the screwing task showed that the exoskeleton could reduce muscle activation (up to 49.6%), perceived effort and frustration, and provide an improved user experience (scored 79.7 out of 100). **Conclusion:** These results indicate that the proposed exoskeleton can guarantee natural movements and provide efficient assistance during overhead work, and thus have the potential to reduce the risk of musculoskeletal disorders. **Significance:** The proposed exoskeleton provides insights into multi-task adaptability and efficient assistance, highlighting the potential for expanding the application of exoskeletons.

Index Terms—Shoulder exoskeletons, musculoskeletal disorders, overhead work, efficient torque generator, ergonomics.

I. INTRODUCTION

WORK-RELATED musculoskeletal disorders (WMSDs) are the main health threats to workers [1], [2]. Shoulder WMSDs have received widespread attention due to their high prevalence (13% of cases) and prolonged absenteeism (23 days) [3]. Overhead work often relates to extreme and awkward shoulder postures [4], which is recognized as a primary contributor [5]. Although robots have been involved in many factory tasks, numerous complex activities that demand human cognition or operate in narrow spaces still require workers [6]. Occupational shoulder exoskeleton (OSE) technology is an available solution to reduce the burden on the shoulder [7].

This work was supported in part by the National Natural Science Foundation of China under Grant 62306083 and the Postdoctoral Science Foundation of Heilongjiang Province of China under Grant LBH-Z22175. (Correspondence author: Baichun Wei, Chunzhi Yi)

Jin Tian and Chifu Yang are with the School of Mechatronics Engineering, Harbin Institute of Technology, Harbin, 150001, China (e-mail: jin.tian@stu.hit.edu.cn; cfyang@hit.edu.cn).

Haiqi Zhu, Baichun Wei, and Chunzhi Yi are with the School of Medicine and Health, Harbin Institute of Technology, Harbin, 150001, China (e-mail: haiqizhu@hit.edu.cn; bcwei@hit.edu.cn; chunzhiyi@hit.edu.cn).

Changjia Lu and Yingjie Liu are with the Emergency Science Research Institute, Chinese Institute of Coal Science, Beijing, 100013, China (e-mail: lusipshan@163.com; liuyingjie@mail.ccrc.ctectg.cn).

Copyright (c) 2021 IEEE. Personal use of this material is permitted. However, permission to use this material for any other purposes must be obtained from the IEEE by sending an email to pubs-permissions@ieee.org.

OSEs can be classified into active, semi-active, and passive categories. In general, active OSEs can provide higher, more precise, and versatile assistive torques [8]–[10]. However, they have larger volumes and higher maintenance costs [11]. As an alternative solution, semi-active OSEs can automatically adjust torque profiles by employing small low-power motors [12], such as the H-PULSE [9], [13]. Compared to active ones, it is more compact and has lower energy consumption while maintaining effectiveness. However, compared to passive ones, the maintenance and manufacturing costs of semi-active OSEs are higher, which would limit their widespread adoption and application. Passive OSEs (POSEs) are characterized by their low cost and lightweight design [14], [15], which provide arm gravity compensation during overhead works without external power sources. Recent studies have demonstrated that wearing POSEs can reduce muscle activation during overhead tasks performed in laboratory and field settings [16]–[18]. Even though POSEs have been commercialized, some pending issues remain, thus impeding user acceptance and assistive efficiency [19].

One of the main issues is the insufficient kinematic compatibility between the exoskeleton and the user [20]. POSEs can be classified based on the presence or absence of an exoskeletal shoulder structure above the human shoulder [11]. Exoskeletons with a rigid structure above the human shoulder, such as the ShoulderX [21] and Airframe [22], typically feature a degree of freedom (DoF) next to the shoulder to follow shoulder flexion/extension (F/E) movements. These exoskeletons are compact and thus are suitable for performing overhead tasks in narrow spaces. However, they may induce collisions between the shoulder and the exoskeleton at high elevation angles, resulting in an insufficient range of motion (ROM). Exoskeletons without a structure above the shoulder, such as the SPM [23] and Exo4Work [24], avoid collisions at high elevation angles. However, they generally incorporate multi-DoF structures in the back to accommodate shoulder movements, which leads to a larger volume. The drawback may result in collisions with the surrounding objects in narrow spaces. In existing exoskeletons, achieving both sufficient ROM and compactness is mutually exclusive. To achieve a balance between them, Junsoo Kim et al. [11] designed an exoskeleton with tilted shoulder structures for assisting overhead tasks. However, it still cannot provide a sufficient ROM for horizontal F/E movements, which may induce a decreased user experience. There is an urgent need for an exoskeleton that can simultaneously provide sufficient ROM and compactness.

Another main issue is the task-specific or individual-specific design, corresponding to a fixed assistive torque profile and thus a fixed assistive region (i.e. the subset of ROM where the exoskeleton can assist), which may not be optimal for other tasks [25], [26]. Overhead tasks relate to different positions, especially different elevation angles of the shoulder (e.g., screwing task of the automobile manufacturing industry [21], [27], [28], aircraft squeeze riveting and sealing tasks [29], [30], the welding task of shipbuilding [11], order picking task [16] and so on). Consequently, various overhead tasks require different optimal torque profiles [13], [24]. In addition, the same task may have different target angles for individuals of different heights, which requires providing personalized torque profiles [31].

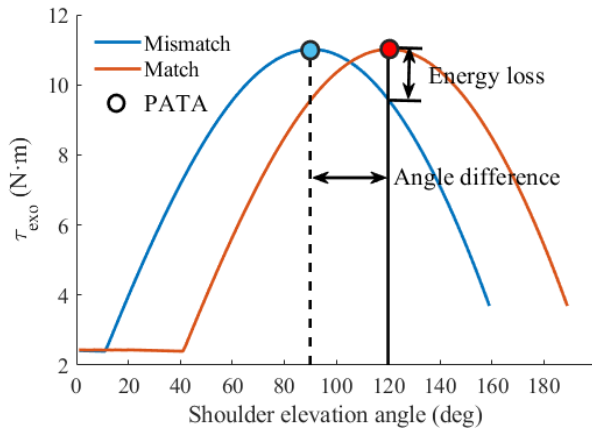


Fig. 1. The torque profiles when there is a match (orange line) or mismatch (blue line) between the PATA and the target angle of the task in an overhead task with a target angle of 120° . Angle difference refers to the discrepancy between the PATA and target angle of the task.

The torque profile should be adaptive to tasks and subjects, essentially characterized by the amplitude and peak assistive torque angle (PATA). The amplitude of the peak assistive torque can be easily tuned by adjusting the extension length of the spring. For example, the MATE can manually change the peak torque by a knob [32], and H-PULSE can adjust the spring length by a spindle drive coupled with a servomotor [9], [13]. The timing of the peak assistive torque ensures that the POSE can provide timely assistance when the torque profile reaches its peak value at specific elevation angles of the shoulder [19]. Fig. 1 depicts the torque profiles when there is a match or mismatch between the PATA and the target angle of the task in an overhead task with a target angle of 120° . When there is a match between them, it ensures timely assistance and reduces energy loss, making it a more efficient assistive strategy. However, current POSEs can only change the PATA through reconstruction, which means they cannot provide torque profiles for different tasks or individuals, i.e., insufficient adaptability [26], [31]. In summary, different tasks and individuals should have different PATAs, lacking in current POSEs. Therefore, an adjustable PATA is needed to enhance task and subject adaptability.

The object of this study is to develop, implement, and preliminarily evaluate a novel POSE for overhead tasks, named HIT-POSE. Our prototype can provide a sufficient ROM of the human shoulder and possess an adjustable PATA, thus adapting to various overhead tasks and individuals. The major contributions of our work are as follows:

(a) We designed a torque generator with adjustable PATA to adapt to different overhead tasks and individuals. To the best of our knowledge, it's the first torque generator that can provide adjustable PATA to achieve more efficient assistance.

(b) We developed an ergonomic shoulder structure through kinematic modeling and simulation, which can guarantee sufficient ROM for the shoulder while remaining compact (without redundant structures in the back), thus reducing the risk of collisions with the environment.

(c) We also investigated how the modulation of the PATA could affect objective and subjective evaluation indicators in overhead tasks via experimental assessment, thus validating the effectiveness of the exoskeleton.

II. SYSTEM DESIGN OF HIT-POSE

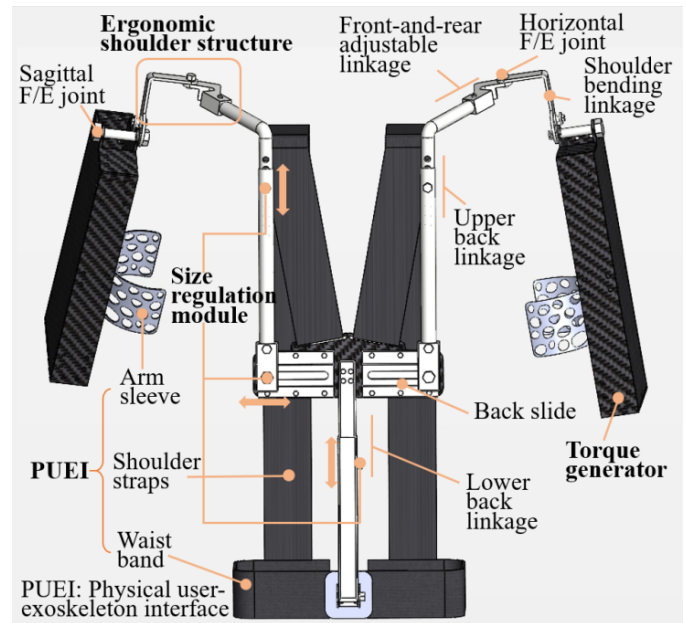


Fig. 2. An overview of HIT-POSE.

A. System Overview

Overhead work is defined as working with hands above acromion or over 60° shoulder flexion or abduction [33]. Therefore, we can define the workspace for overhead tasks as the sagittal flexion of the shoulder with 60° to 168.8° (the maximum shoulder flexion angle for healthy adult male [34]), abduction angle of the shoulder greater than 60° , and horizontal flexion of the shoulder with 0° to 162.2° (the maximum shoulder horizontal flexion angle for healthy adult male [11]). In addition, the total weight of the exoskeleton should be less than 5kg [19].

HIT-POSE is designed to compensate for shoulder gravitational torque while providing sufficient ROM for the shoulder, as illustrated in Fig. 2. The total weight of the device 2.8 kg. It is suitable for people with a back length of 43.6-66.6 cm and a shoulder width of 29.6-45.6 cm, and the volume of our device is 22cm \times 48cm \times 15cm. HIT-POSE comprises four main modules: (a) the ergonomic shoulder structure, (b) the torque generator with adjustable PATA, (c) the physical user-exoskeleton interface (PUEI), and (d) the size regulation module.

B. Ergonomic Shoulder Structure

We conducted kinematic modeling of the exoskeleton and the user and simulated ROM to select optimal design parameters. The proposed exoskeleton has a horizontal F/E joint above the shoulder and lacks redundant structures in the back. Our object here is to provide sufficient ROM for the shoulder, especially at high elevation angles.

The intersection of the rotational axes of the sagittal and horizontal F/E joints is considered the center of the shoulder of the exoskeleton (CSE), as shown in Fig. 3. The CSE is close to the center of the shoulder of the user (CSU), enabling the torque generator to trace the shoulder movements with a relatively low DoF (Fig. 3). However, it does not coincide with the CSU, indicating the necessity to find the optimal design parameters. As explained in [35] and [36], the shoulder motion can be observed with humeral elevation and posterior displacement of the CSU.

Fig. 3 demonstrates the extracted design parameters (ϕ , d_v , d_b), which can reconfigure the shoulder structure. We defined the ϕ -

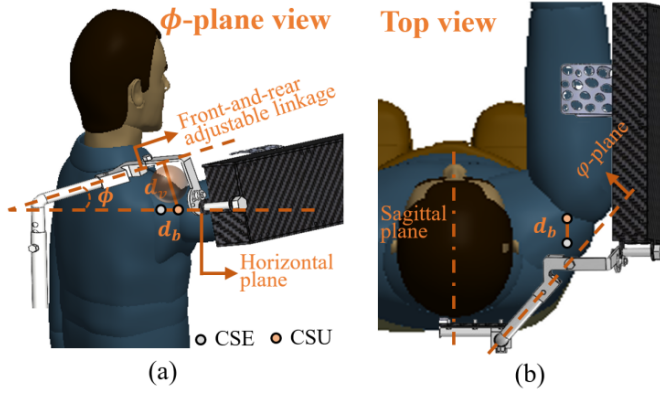


Fig. 3. Definition of the design parameters (ϕ , d_v , d_b). (a) ϕ and d_v are defined from the ϕ -plane view, the orange clear orb represents the room between the CSU and the front-and-rear adjustable linkage. (b) d_b is defined from the top view.

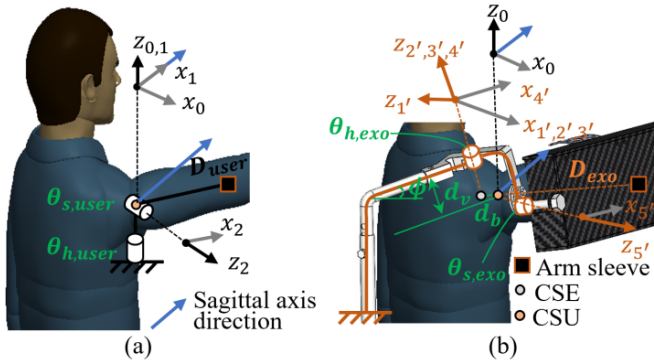


Fig. 4. Kinematic models. (a) The user. (b) The exoskeleton.

plane as the plane containing the front-and-rear adjustable linkage and perpendicular to the horizontal plane (Fig. 3). Viewed from the ϕ -plane, the pitch angle (ϕ) is the angle between the front-and-rear adjustable linkage and horizontal plane, and the vertical distance (d_v) refers to the perpendicular distance from the CSU to the front-and-rear adjustable linkage, as presented in Fig. 3a. Bias distance d_b is defined as the distance between the CSE and CSU from the top view (Fig. 3b). ϕ and d_v can determine the configuration of the front-and-rear adjustable linkage and shoulder bending linkage, respectively. d_b can be regulated by adjusting the length of the front-and-rear adjustable linkage, to adapt to different users and ensure comfort. The orange clear orb (Fig. 3a) can be enlarged by increasing ϕ and d_v , provided for humeral elevation and avoiding collision at high elevation angles. Increasing d_b shifts CSE posteriorly, compensating for the displacement of the CSU during shoulder movement. Overall, a proper combination of design parameters (ϕ , d_v , d_b) can increase the user's ROM when wearing the exoskeleton.

To better explore the effect of design parameters on ROM, the kinematic analyses were conducted, as shown in Fig. 4. In this study, we only consider 2-DoFs of the user's shoulder, a horizontal and

TABLE I. DH PARAMETERS OF THE USER

| | α_{i-1} | a_{i-1} | d_i | θ_i |
|-------------------------|----------------|------------|-------|--------------------------|
| 1'($\theta_{h,user}$) | 0 | 0 | 0 | $\pi/2+\theta_{h,user}$ |
| 2'($\theta_{s,user}$) | $-\pi/2$ | 0 | 0 | $-\pi/2+\theta_{s,user}$ |
| Arm sleeve | 0 | D_{user} | 0 | 0 |

TABLE II. DH PARAMETERS OF THE EXOSKELETON

| | α_{i-1} | a_{i-1} | d_i | θ_i |
|-----------------------|----------------|-----------|--------|------------------------------|
| 1(d_b) | $\pi/2$ | 0 | d_b | 0 |
| 2(ϕ , d_v) | $-\pi/2+\phi$ | 0 | d_v | 0 |
| 3($\theta_{h,exo}$) | 0 | 0 | 0 | $\pi/2+\theta_{h,exo}$ |
| 4(d_v) | 0 | 0 | $-d_v$ | 0 |
| 5($\theta_{s,exo}$) | $-\pi/2$ | 0 | 0 | $-\phi-\pi/2+\theta_{s,exo}$ |
| Arm sleeve | 0 | D_{exo} | 0 | 0 |

Simulation I Calculate the user's ROM when wearing the exoskeleton

| Input | $\theta_{h,exo}$, $\theta_{s,exo}$, ϕ , d_v , d_b , D_{exo} , D_{user} |
|--------|--|
| Output | ROM simulation results |
| 1: | Calculating the position of the arm sleeve (p_x , p_y , p_z) via forward kinematics of the exoskeleton; |
| 2: | Solving $\theta_{h,user}$ and $\theta_{s,user}$ using inverse kinematics of the user and position of arm sleeve (p_x , p_y , p_z); |
| 3: | Checking collision between the exoskeleton and user; |
| 4: | Obtain the non-collisional joint angles of the user. |

sagittal F/E DoF, whose angles were denoted by $\theta_{h,user}$ and $\theta_{s,user}$ (Fig. 4a). Similarly, the exoskeleton's shoulder has 2-DoFs, whose angles are denoted by $\theta_{h,exo}$ and $\theta_{s,exo}$ (Fig. 4b). These four angles represent the ROM for both the human and the exoskeleton. D_{user} and D_{exo} represent the distances from the CSU and CSE to the arm sleeve (Fig. 4), respectively.

Tables I and II demonstrate the specific Denavit-Hartenberg (DH) parameters of both models. The association between the two models is that the coordinate origin (the CSU in Fig. 4) and arm sleeve are in the same location. Based on the characteristics, we formulated a simulation pipeline via the analytical method to calculate the user's ROM when wearing the exoskeleton, as displayed in Simulation I. Notably, the principle for checking collisions is that the angles of the user cannot be greater than that of the exoskeleton.

A previous study has stated that the CSU is about 2 cm below the acromion [37]. Additionally, the CSU is vertically displaced by around 6 cm during shoulder movement [38]. Such prior knowledge provides a basis for choosing the value of d_v . We provide seven sets of design parameters and their ROM simulation results, as shown in Fig. 5. The area below each set of curves is the corresponding ROM. When $\theta_{h,user}=0$, the maximum value of $\theta_{s,user}$ is obtained. The ROM can be enlarged by increasing ϕ and d_v , thus preventing collisions at high elevation angles. To maximize the user's ROM, ϕ and d_v were set to 15° and 80 mm, respectively. As d_b increases, the CSE moves toward the posterior of the user, causing increased ROM, but too large d_b will lead to discomfort. Eventually, we take the penultimate set ($\phi=15^\circ$, $d_v=80\text{mm}$, $d_b=10\text{mm}$) as the final design parameters. In this set, the ROM is sufficient to ensure the user's natural movement and complete overhead tasks.

C. Torque Generator with Adjustable PATA

The torque generator is composed of a sagittal F/E joint bar, PATA adjustable module, parallel spring group, spring pretension tuning module, carbon fiber shell, and five pulleys with inner bearings (Fig. 6a). A wire rope of 1mm diameter connects the parallel spring group to pulley 2. The pulleys 3 and 4 can be moved vertically through the guide rail, resulting in the adjustable PATA. The 8-shaped loop with a rotational DoF connects the parallel spring group with the spring pretension tuning module. It ensures that the parallel spring group does not experience axial rotation when screwing the spring pretension tuning module. Three identical springs (i.e., $L_s=L_{AB}=L_{CD}=L_{EF}$) are installed in the parallel spring group to obtain a high energy storage capability.

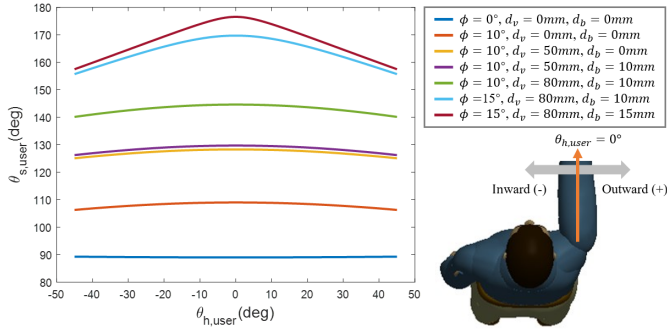


Fig. 5. ROM simulation results of the user with seven sets of design parameters (ϕ , d_v , d_b).

The assistive principle is to store or release the elastic potential energy of springs as the arm is lowered or raised, respectively. Since the torque generator follows the arm movement via an arm sleeve, it can be considered that the sagittal F/E angle of the exoskeleton ($\theta_{s,exo}$) is approximately equal to that of the user ($\theta_{s,user}$). The generated assistive torque (τ_{exo}) can be formulated as:

$$\tau_{exo} = F_s L_{exo}. \quad (1)$$

where F_s is the tension generated by springs, and L_{exo} denotes the perpendicular distance between point O and the wire rope (Fig. 7a). Furthermore, F_s can be expressed as:

$$F_s = K \Delta L. \quad (2)$$

where K is the stiffness of the parallel spring group, which is triple that of a single spring (k_s), i.e., $K=3k_s$, and ΔL represents the total extension length of the parallel spring group. Fig. 7b displays the generated assistive torque (τ_{exo}) under a set of design parameters (can be found in Table III), along with L_{exo} and ΔL . To derive the assistive torque, the total extension length of the parallel spring group (ΔL) should be formulated as a function of the sagittal F/E angle of the exoskeleton ($\theta_{s,exo}$). During the shoulder movement, the extension length of the parallel spring group can be considered equivalent to the length change of the wire rope between points A' and B', as they are connected in series. Therefore, the total extension length of the parallel spring group (ΔL) can be expressed as:

$$\Delta L(\theta_{s,exo}) = L_{A'B'}(\theta_{s,exo}) - L_{A'B'}(\max(\theta_{s,exo})) + L_i. \quad (3)$$

where $L_{A'B'}$ is the length of the wire rope routed from A' to B' (Fig. 6b and 6c). A' and B' are the starting and ending points of the wire rope that attach to pulley 2 and pulley 4, respectively, and L_i denotes the initial extension length caused by the spring pretensioning module. The minimum value of $L_{A'B'}$ is obtained at the maximum value of $\theta_{s,exo}$, which is set to 170° due to the safety limit.

Based on (1) to (3) and Fig. 7b, the main factor affecting PATA is L_{exo} , rather than ΔL , as it is monotonically decreasing. The primary parameters affecting the phase shift of L_{exo} are α and β , denoting the angles of pulleys 2 and 3, as shown in Fig. 6b and 6c. When α decreases or β increases, PATA would decrease and thus the phase of L_{exo} curve would shift to the left (Fig. 7a and 7b). The assistive torque would be influenced by L_{exo} and also have a phase shift (as shown in Fig.1). To better investigate the trend of PATA, when $\alpha=\beta=0$, we defined the PATA as a reference, denoted by θ_0 . The PATA (θ_{PATA}) can be derived as:

$$\theta_{PATA} = \theta_0 + \alpha - k\beta. \quad (4)$$

$$\theta_0 = 90 - \arctan\left(\frac{r}{r_2}\right). \quad (5)$$

TABLE III. THE EFFECTS OF PARAMETERS (α , β , r_1 , r_2 , r_3 , L_i) ON TORQUE ASSISTIVE AND PATA IN BOTH PHASES

| Requirement | Parameter | Value |
|-------------------|-----------|------------|
| | K | 12N/mm |
| Peak torque | L_i | 30mm |
| | r_1 | 20mm |
| | r_2 | 40mm |
| Torque at phase I | r_3 | 3mm |
| Critical angle | α | 40° |

TABLE IV. THE EFFECTS OF PARAMETERS (α , β , r_1 , r_2 , r_3 , L_i) ON TORQUE ASSISTIVE AND PATA IN BOTH PHASES

| Parameter | Phase I | Phase II | |
|-----------|-----------------|----------------|----------------|
| | τ_{exo} | τ_{exo} | PATA |
| α | NI ^a | N ^b | P ^c |
| β | NI | P | N |
| r_1 | NI | P | NI |
| r_2 | NI | NI | NI |
| r_3 | P | NI | NI |
| L_i | P | P | NI |

^a: No Impact; ^b: Negative; ^c: Positive.

where r is the radius of pulley 3, which is 7mm in this paper, thus θ_0 is 80° ; and k is a variable positive coefficient around 1, due to the nonlinear effect of ΔL on τ_{exo} . To change the PATA for adapting different overhead tasks, we adjusted β by moving pulleys 3 and 4 along the guide rail, the relationship between β and PATA can be found in Fig. 8. We employed α to control the maximum sagittal F/E joint angle ($\theta_{s,exo}$). α can be adjusted by changing the mounting position of pulley 2 through the pre-drilled holes, and its mappings to the maximum of $\theta_{s,exo}$ are indicated by the dotted line in Fig. 9e.

D. Parameters Impact on Torque Profiles

In this subsection, we analyzed the impact of design parameters on the peak value and PATA of the torque profile and conducted a simulation of torque profiles. Table III shows the parameters of the torque generator.

As visualized in Fig. 6b and 6c, the generated assistive torque can be divided into two phases based on whether the wire rope is routed to the sagittal F/E joint bar. When the wire rope is attached to the sagittal F/E joint bar (Phase I, Fig. 6b), the assistive torque remains low to avoid hindering normal activities like walking, corresponding to the low assistance zone (Fig. 7b). In contrast, when the wire rope is detached from the sagittal F/E joint bar (Phase II, Fig. 6c), the assistive torque increases rapidly to provide effective assistance for the target task, corresponding to the high assistance zone (Fig. 7b). We defined the critical angle for switching between phases I and II as θ_c (Fig. 7a), which is dependent on α and β (Fig. 6b and 6c). As α increases or β decreases, θ_c increases (Fig. 9e - 9f). The wire rope coupled with the sagittal F/E joint bar formulates a passive clutch mechanism that allows for switching between low and high assistance zones. If there is no sagittal F/E joint bar (i.e., orange dotted line in Fig. 6b), the torque generator will pull the arm backward, which poses a safety hazard to the user. It is worth noting that this mechanism also provides a torque of approximately 2 N·m, although it is much smaller than the peak assist torque, it may still reduce the user's acceptance of the exoskeleton.

L_{exo} and $L_{A'B'}$ can be geometrically calculated in the two phases. Based on (1) to (3), the peak value of the assistive torque increases with the stiffness (K) and initial extension length (L_i) of the parallel spring group in both phases. In phase I, the primary parameter affecting L_{exo} and $L_{A'B'}$ is r_3 , the radius of the sagittal F/E joint

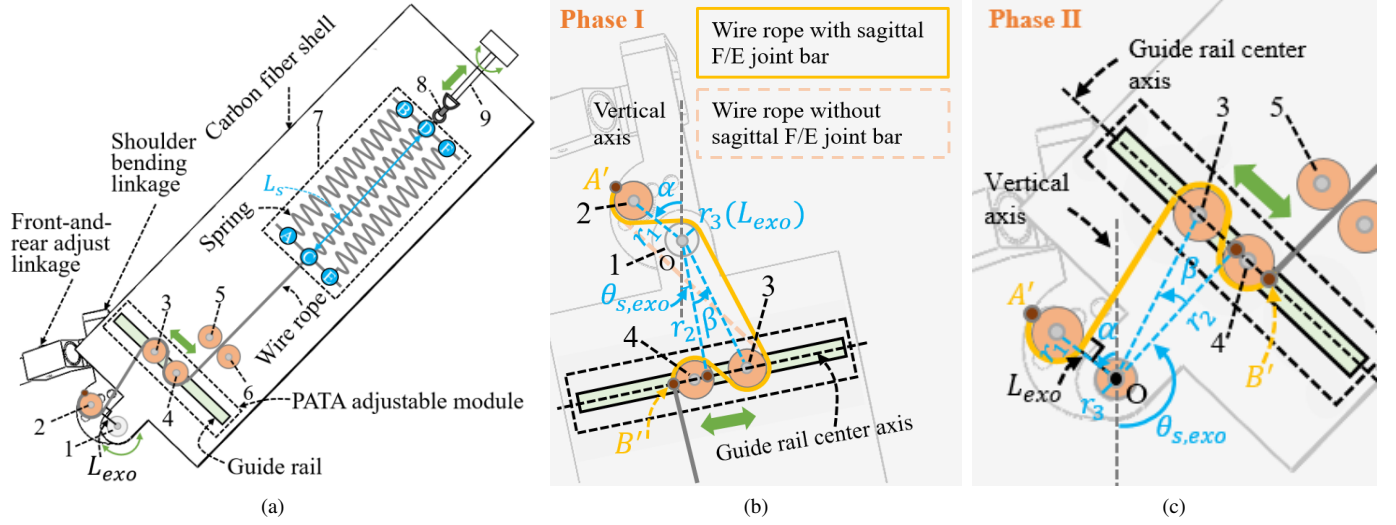


Fig. 6. The overall structure and design parameters of the torque generator with adjustable PATA. (a) Components of the torque generator. (b) Torque generator with parameters $(\alpha, \beta, r_1, r_2, r_3)$ after the wire rope is attached to the sagittal F/E joint bar (Phase I). (c) Torque generator with parameters $(\alpha, \beta, r_1, r_2, r_3)$ before the wire rope is attached to the sagittal F/E joint bar (Phase II). 1: Sagittal F/E joint bar. 2: Pulley fixed to the shoulder bending linkage. 3-6: Pulleys fixed to the carbon fiber shell. 7: Parallel spring group. 8: 8-shaped loop. 9: Spring pretension tuning module. L_{exo} : the force arm of the assistive torque.

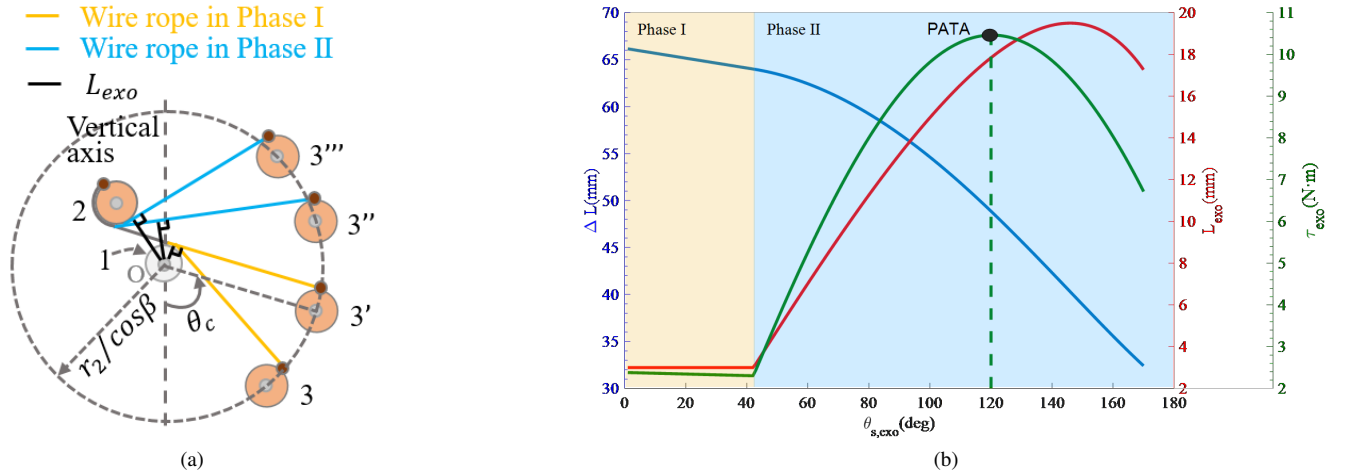


Fig. 7. The principal of the assistive torque profile. (a) Overlapped location configurations of the force arm L_{exo} , θ_c is the critical angle between phases I and II, r_2 is the distance between the guide rail and the sagittal F/E joint, β is the angle of pulley3, as shown in Fig. 6b. (b) Torque profile τ_{exo} along with the force arm L_{exo} and total extension length of the parallel spring group ΔL . The area shaded in light orange is Phase I, and that in light blue is Phase II.

bar. As r_3 increases, L_{exo} and $L_{A'B'}$ increase, resulting in an increase in assistive torque within the low assistance zone. In phase II, the primary parameters affecting L_{exo} and $L_{A'B'}$ are α, β, r_1 , where r_1 represents the distance between pulley 2 and the sagittal F/E joint. As r_1 increases, L_{exo} and $L_{A'B'}$ increase, causing an increase in the peak value of the assistive torque. When α decreases or β increases, $L_{A'B'}$ increases, leading to an increase in the peak value of the assistive torque, and the impact on L_{exo} has been stated in subsection C. We also extracted and tested r_2 , the distance between the guide rail and the sagittal F/E joint, as a design parameter. The result showed that it essentially has no significant impact on the peak or phase of the assistive torque, allowing us to choose an appropriate value according to the requirements of the design space. Table IV

summarizes the effects of the parameters $(\alpha, \beta, r_1, r_2, r_3, L_i)$ on the assistive torque and PATA.

Fig. 9 demonstrates how the parameters affect the assistive torque profiles through simulations with an ideal situation (i.e., no deformation and friction). The simulation results in Fig. 9 are in accord with our previous analyses. In particular, the parameters L_i, α and β can be easily adjusted, and K can be easily changed by replacing the spring. Consequently, this implies that the main characteristics of the torque profile can be tuned by reconfiguring the exoskeleton (i.e. by tuning the pre-tension of springs or the mounting position of pulley 2), rather than reconstructing it. As far as we know, this is the first exoskeleton that can simultaneously modify these characteristics of the torque profile without the need of reconstruction.

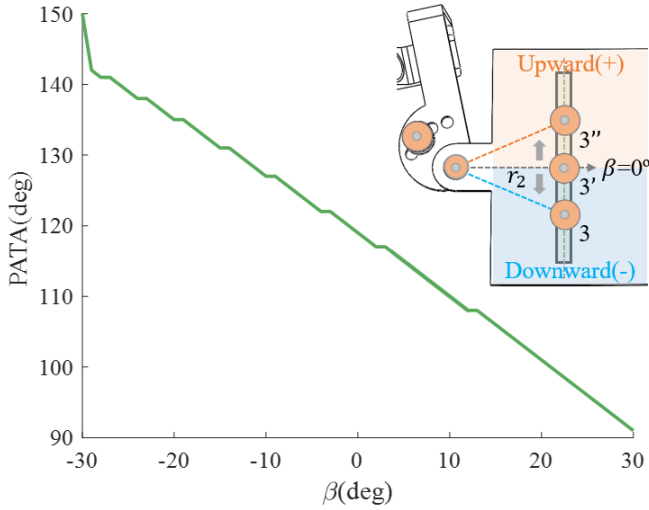


Fig. 8. The relationship between β and PATA.

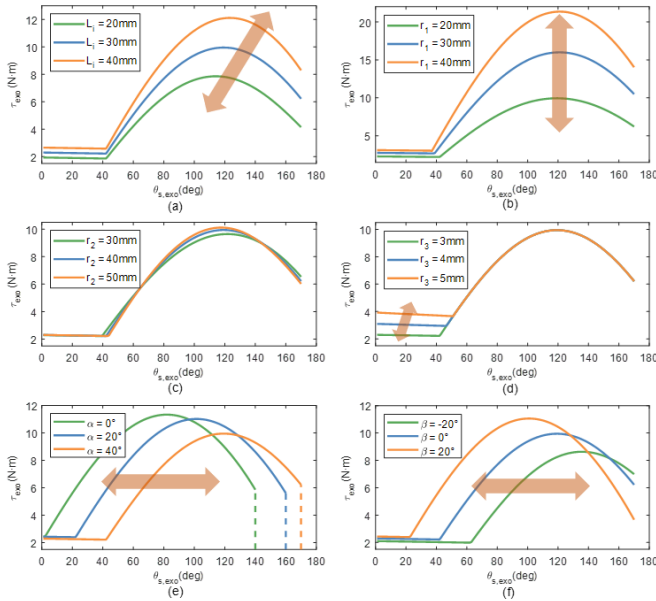


Fig. 9. The simulated assistive torque (τ_{ext}) profiles were obtained via tuning of the assistive parameters. (a) L_i , (b) r_1 , (c) r_2 , (d) r_3 , (e) α , (f) β .

E. PUEI and Size Regulation Module

The PUEI contains a lower back linkage and all components that attach the exoskeleton to the user, e.g., shoulder straps, chest buckles, and waist band. These flexible fabrics ensure a compliant human-exoskeleton interface. Furthermore, the lower back linkage is made of aluminum alloy, which transmits the force compensated by the torque generator to the waist.

The size regulation module is designed to accommodate diverse ergonomic needs while ensuring both comfort and safety. The height and width of the back are adjustable through upper and lower back linkages, as well as lateral back slides. Additionally, the flexible fabric allows for precise tightening of the exoskeleton around the user's waist, back, and arms.

III. EXPERIMENTAL EVALUATIONS

Two experimental sessions were conducted to verify the HIT-POSE has (a) a sufficient ROM (session 1), and (b) an ability and

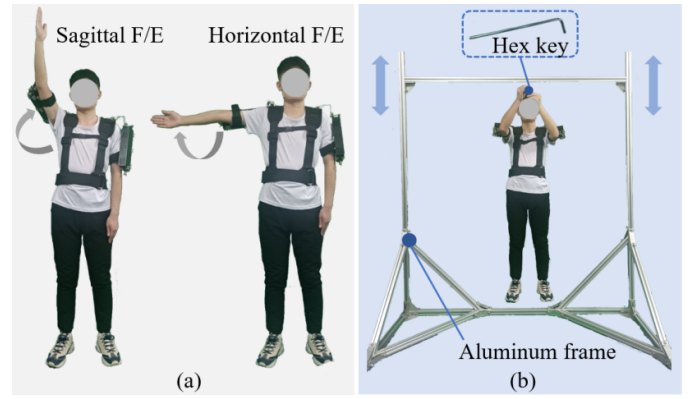


Fig. 10. Experimental tasks. (a) Shoulder movements in session 1. (b) Screwing task in session 2.

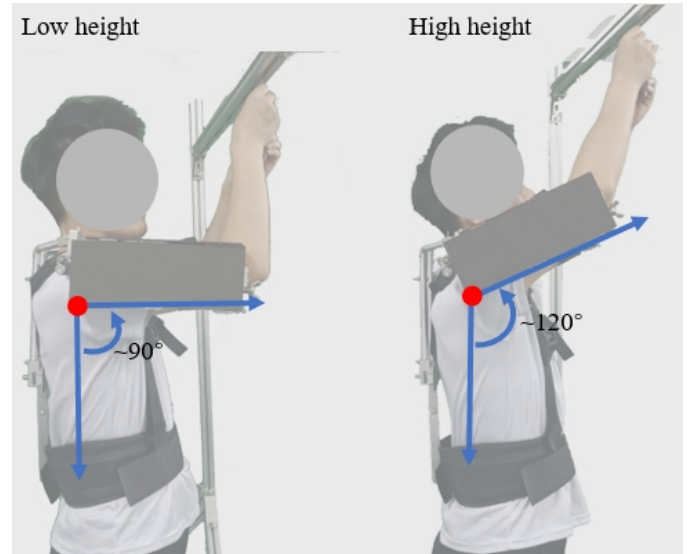


Fig. 11. The definition of the low (left) and high (right) heights.

adaptability to assist different overhead tasks (session 2).

A. Participants

Two separate groups of participants were recruited for this study. Five healthy subjects participated in session 1 (all male, all right-handed, age: 24.1 ± 1.64 years, height: 173.8 ± 3.27 cm, weight: 70 ± 9.06 kg), and ten healthy subjects participated in session 2 (all male, all right-handed, age: 25.1 ± 2.0 years, height: 177 ± 4.3 cm, weight: 68.3 ± 9.3 kg). All participants had no prior experience with the exoskeleton and signed an informed consent before the experiment. The experimental protocol received approval from the Chinese Ethics Committee of Registering Clinical Trials (ChiECRCT20200319).

B. Data Recordings

ROM of the right-side shoulder was measured by the motion capture system (100Hz, VICON, Oxford Metrics, Oxford, UK). Muscular activities were monitored using the surface EMG electrodes (1111Hz, Delsys Inc., Natick, MA, USA). Meanwhile, acceleration signals were recorded through an IMU (148Hz, Delsys Inc., Natick, MA, USA). Notably, the motion capture system did not work simultaneously with EMG. Thus, we did not synchronize them through a trigger.

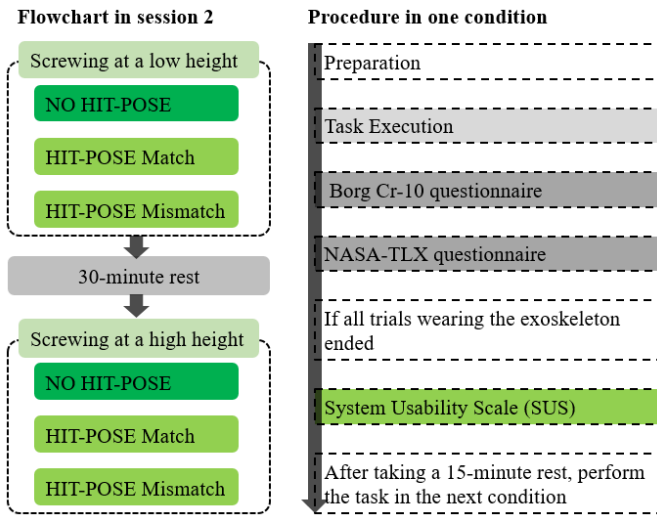


Fig. 12. The experimental flowchart (left) in session 2 and procedure in one condition (right). The order of the conditions and tasks is randomized.

C. Experimental Tasks

In session 1, participants were directed to maximize sagittal and horizontal F/E movements, at a self-selected constant pace, as shown in Fig. 10a. In session 2, participants were guided to screw the M6 bolts with a hex key (mass: 8.6 g), as shown in Fig. 10b. Nuts were embedded in an aluminum frame, which was set to two heights: low height was defined as hand with the shoulder at about 90° , and high height was defined as hand with the shoulder at about 120° (Fig. 11).

D. Procedure

Before the experiment, participants were introduced to the experimental paradigm and familiarized with HIT-POSE and tasks. In session 1, tasks were performed under two conditions: without the exoskeleton (NO HIT-POSE) and with the exoskeleton (HIT-POSE). Each participant completed six trials: three in each condition, with each trial consisting of five movements and lasting about 30 seconds. In session 2, the exoskeleton was configured for screwing at low and high heights (Fig. 12). Both configurations had the same peak torque but different PATAs for the respective heights. A match between the PATA and the task angle was defined as HIT-POSE Match; otherwise, it was HIT-POSE Mismatch. Each task was performed under three conditions: NO HIT-POSE, HIT-POSE Match, and HIT-POSE Mismatch (Fig. 12), with each trial lasting 2 minutes per condition.

Surface EMG electrodes were placed unilaterally on the right-side muscles according to SENIAM guidelines [39]: anterior deltoid (AD), middle deltoid (MD), posterior deltoid (PD), bicep brachii (BB), pectoralis major (PM), trapezius (TR), latissimus dorsi (LD), erector spinae (ES). Additionally, an IMU was placed on the right wrist to measure the acceleration. Then, the EMG signals were normalized for each participant and task using the maximal amplitude of each muscle during NO HIT-POSE conditions [40]–[42]. The order of conditions and tasks was randomized across participants to avoid order effects. After each trial, participants completed the NASA-TLX [43] to assess perceived workload (PW) and the Borg CR-10 [44] for rating perceived exertion (RPE). After all exoskeleton trials, they completed the System Usability Scale (SUS) [45]. Fig. 12 presents the experimental procedure for session 2.

TABLE V. MEASURED ROM WITHOUT AND WITH HIT-POSE

| Condition | Maximum sagittal F/E angle (deg) | Maximum horizontal F/E angle (deg) |
|-------------|----------------------------------|------------------------------------|
| NO HIT-POSE | 165.13 ± 2.15 | 159.74 ± 6.27 |
| HIT-POSE | 164.46 ± 2.21 | 158.28 ± 7.20 |

E. Data and Statistical Analysis

In session 1, mean values of the maximum sagittal and horizontal F/E angles were calculated using shoulder angles measured by VICON and corresponding hand workspace were calculated using the position of the reflective point on hand measured by VICON among all participants in NO HIT-POSE and HIT-POSE conditions. In session 2, acceleration signals were resampled to 1111Hz, and variances were calculated using a 30ms sliding window. A set variance threshold determined the start and end times of each trial. EMG signals were processed to compute the linear envelopes by setting them to zero-mean, applying band-pass filter (4th, 20-350Hz), full-wave rectification, low-pass filter (6Hz), and normalization. For each trial, the root mean square (RMS) of each muscle was obtained from the linear envelope via a 30ms time sliding window during the phase of task execution.

Statistical analyses were used to assess the effectiveness of the exoskeleton in reducing muscle activations and subjective evaluation indicators (i.e., RPE and PW scores). The Shapiro-Wilk test was employed to check data normality. If the normal distribution was not satisfied, the non-parametric analysis of variance (ANOVA) was conducted to check for across-condition differences, otherwise, the parametric ANOVA was applied. A post-hoc analysis was conducted when a significant effect was observed. Statistical significance was concluded when $p < 0.05$.

IV. RESULTS

A. ROM

Table V reports measured ROM averaged among all participants. No significant differences were observed between conditions. The absolute error between the maximum value (169.71°) of the penultimate set in the simulation of Fig. 5 and the maximum sagittal F/E angle (164.46°) in HIT-POSE condition of the experiment was 5.25° . Fig. 13 shows the averaged hand workspace (normalized by the arm length of each subject) of the maximum sagittal and horizontal F/E angles among all participants in both conditions. In both movements, the coordinate origin is the hand's position in the neutral posture before movements. The positive x-axis points to the right side of the body, the positive y-axis points forward, and the positive z-axis points upward. There was no significant statistical difference between conditions for both tasks.

B. Muscular Activations

For all monitored muscles, statistically significant interactions were found in both conditions, as shown in Table VI. Fig. 14 demonstrates the results of muscular activations from pairwise comparisons. In HIT-POSE Match conditions for both tasks, significantly decreased muscular activations in all monitored muscles were found compared to NO HIT-POSE condition. For screwing at a low height, the muscular activations of MD, PD, BB, PM, and LD muscles in HIT-POSE Match condition were significantly reduced compared to that in HIT-POSE Mismatch condition; in addition, the muscular activation of the BB muscle in HIT-POSE Mismatch condition was also significantly reduced compared to that in NO HIT-POSE condition. For screwing at a high height, AD, MD, PD, and PM muscles in

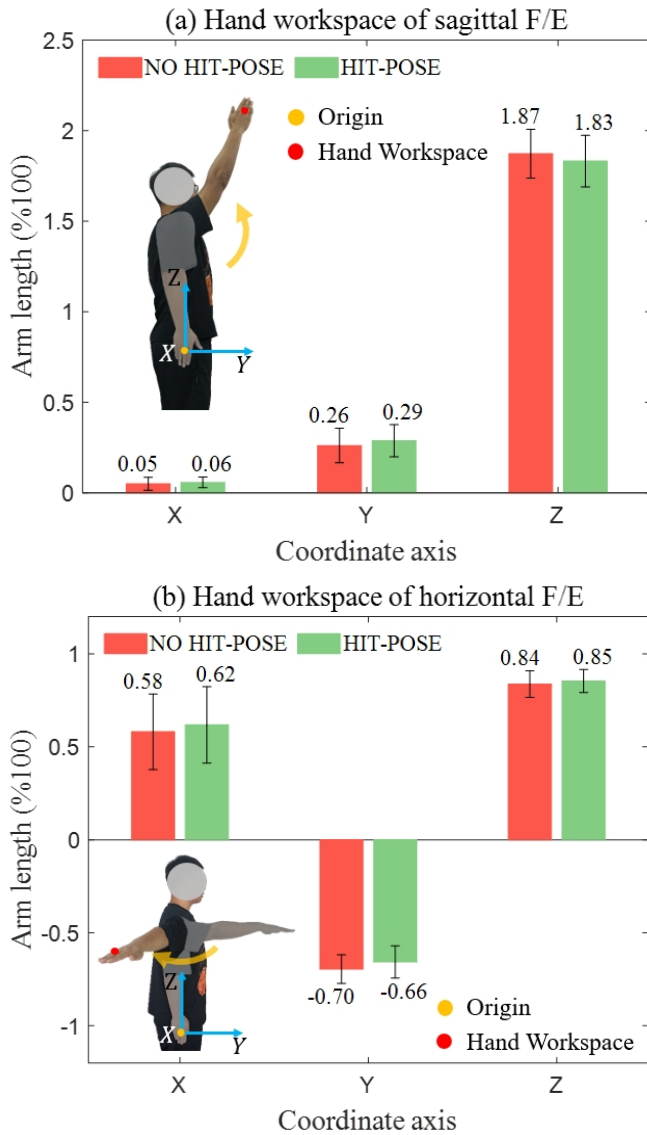


Fig. 13. Averaged hand workspace (normalized by the arm length of each subject) of the maximum sagittal and horizontal F/E angles among all participants in both conditions. (a) Hand workspace of sagittal F/E, (b) Hand workspace of horizontal F/E. The error bar represents the mean \pm standard deviation.

HIT-POSE Match condition exhibited significantly decreased EMG activations compared to that in HIT-POSE Mismatch condition; moreover, BB and TR muscles in HIT-POSE Mismatch condition exhibited significantly decreased EMG activations compared to that in NO HIT-POSE condition.

As shown in Table VII, for both tasks in HIT-POSE Match conditions, the absolute percentage reduction was above 15% (highest at 22.9% and 23.8% for AD in screwing at low and high heights, respectively), and the relative percentage reduction was above 30% (highest at 48.3% for AD in screwing at a low height and 49.6% for BB in screwing at a high height). For both tasks in HIT-POSE Mismatch conditions, the absolute percentage reduction was above 5% (highest at 11.9% for AD in screwing at a low height, and 11.3% for BB and TR in screwing at a high height), and the relative percentage reduction was above 9% (highest at 24.3% for AD in screwing at a low height and 27.7% for BB in screwing at a high

TABLE VI. F AND P-VALUES OF THE ANOVAS ON THE MUSCULAR ACTIVATIONS DURING THE TWO TASKS.

| Muscles | Screwing at a low height | | Screwing at a high height | |
|---------|--------------------------|---------|---------------------------|---------|
| | F-value | P-value | F-value | P-value |
| AD | 11.65 | 0.0006 | 13.03 | 0.0003 |
| MD | 16.84 | 0.0001 | 12.33 | 0.0004 |
| PD | 18.75 | 0.0000 | 19.91 | 0.0000 |
| BB | 13.75 | 0.0002 | 13.25 | 0.0003 |
| PM | 11.23 | 0.0007 | 25.60 | 0.0000 |
| TR | 10.08 | 0.0012 | 11.85 | 0.0005 |
| LD | 10.69 | 0.0009 | 8.10 | 0.0031 |
| ES | 12.00 | 0.0005 | 11.61 | 0.0006 |

TABLE VII. REDUCTION PERCENTAGE (%) OF MUSCLE ACTIVATIONS WHEN WEARING HIT-POSE.

| Muscles | Screwing at a low height | | Screwing at a high height | |
|---------|--------------------------|-----------------------|---------------------------|-----------------------|
| | HIT-POSE Match (%) | HIT-POSE Mismatch (%) | HIT-POSE Match (%) | HIT-POSE Mismatch (%) |
| AD | 22.9 48.3 | 11.5 24.3 | 23.8 48.5 | 10.6 21.6 |
| MD | 15.6 30.3 | 6.5 12.5 | 19.5 37.9 | 8.2 15.8 |
| PD | 18.5 35.6 | 7.0 13.5 | 23.3 44.7 | 8.9 17.1 |
| BB | 15.5 41.9 | 7.6 20.6 | 20.1 49.6 | 11.3 27.7 |
| PM | 19.0 43.4 | 5.5 12.5 | 17.9 31.9 | 5.4 9.6 |
| TR | 19.6 40.9 | 8.8 18.2 | 20.2 42.2 | 11.3 23.6 |
| LD | 17.4 47.0 | 7.6 20.6 | 15.7 42.5 | 7.2 19.6 |
| ES | 15.9 43.3 | 8.0 21.8 | 17.0 43.6 | 8.3 21.4 |

A|B: A and B denote absolute and relative percentage reduction with respect to NO HIT-POSE condition, respectively.

height). For the same muscle in the same task, the absolute and relative decreases in HIT-POSE Match conditions are approximately double those in HIT-POSE Mismatch conditions.

C. Subjective Feedback

For RPE scores, statistically significant interactions were found in both conditions ($F = 14.58$, $p = 0.0002$ for low height; $F = 10.55$, $p = 0.0009$ for high height). Fig. 15 shows the RPE scores averaged across participants from pairwise comparisons. In HIT-POSE Match conditions for both tasks, RPE scores showed a significant difference relative to the other two conditions. For physical demand, effort, and frustration aspects of NASA-TLX, statistically significant interactions were found in both conditions (Physical Demand: $F = 5.52$, $p = 0.0135$ for low height; $F = 5.08$, $p = 0.0179$ for high height. Effort: $F = 7.76$, $p = 0.0037$ for low height; $F = 6.85$, $p = 0.0061$ for high height. Frustration: $F = 6.34$, $p = 0.0082$ for low height; $F = 4.08$, $p = 0.0345$ for high height). For both tasks in HIT-POSE Match conditions, significant differences were found in physical demand, effort, and frustration compared to NO HIT-POSE conditions (Fig. 16). In addition, the average SUS score was 79.7 ± 5.9 .

V. DISCUSSION

A. Kinematics Compatibility

HIT-POSE is equipped with an ergonomic shoulder structure to ensure sufficient ROM for the user. This implies favorable kinematics compatibility, which has a profound impact on the exoskeleton's usability and user acceptance. Typically, some passive shoulder exoskeletons integrate a multi-DoF chain or simplified two-link hinge to increase the ROM, such as the SPM [23] and HUST-EV [46]. However, they may collide with nearby objects easily due to the large volume and protrusions. In addition, the design parameters were fixed, thus lacking reconfigurability. This reduces the adaptability and increases the manufacturing costs of the exoskeleton.

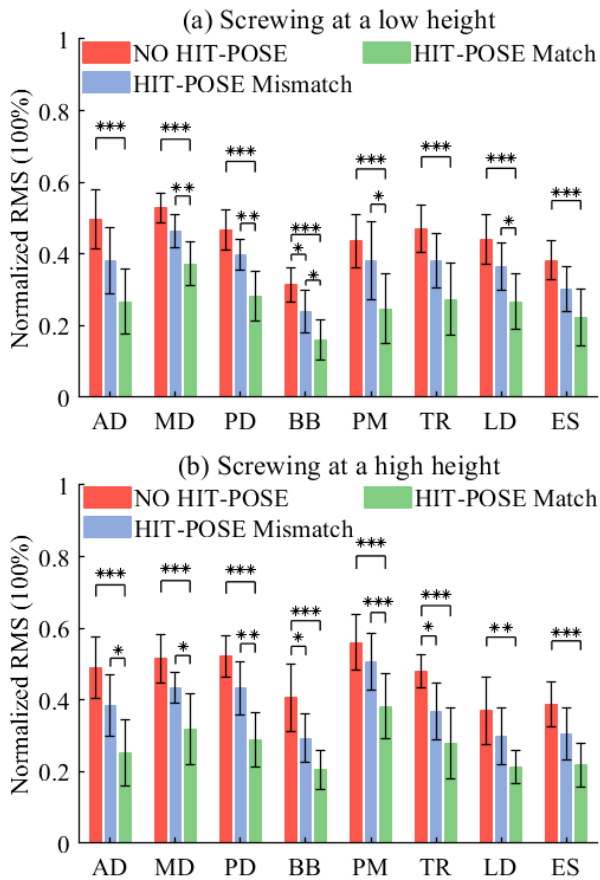


Fig. 14. Muscular activations within different conditions for two tasks from pairwise comparisons. (a) Screwing at a low height. (b) Screwing at a high height. The error bar represents the mean \pm standard deviation. *: $p < 0.05$; **: $p < 0.01$; ***: $p < 0.001$.

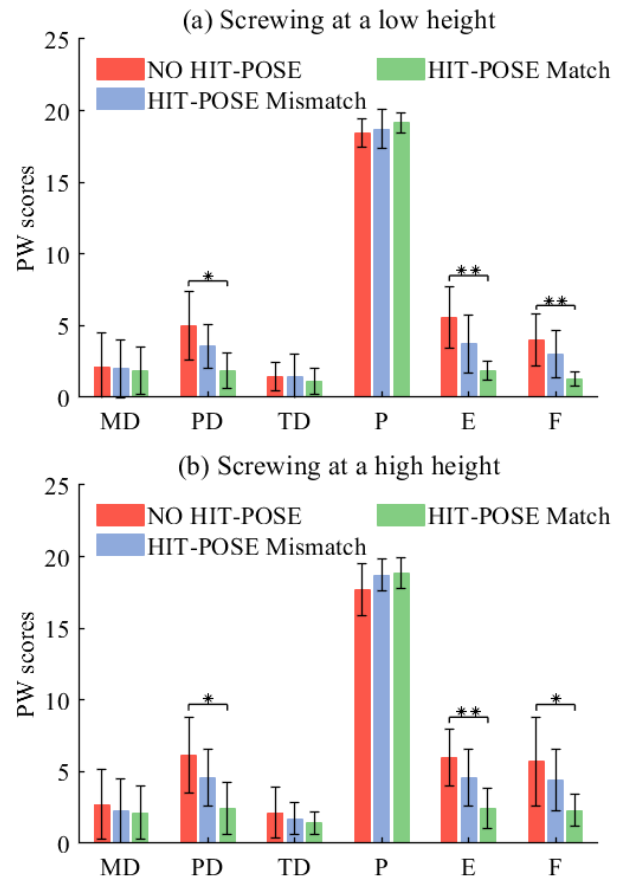


Fig. 16. PW scores for each task among the three conditions from pairwise comparisons. (a) Screwing at a low height. (b) Screwing at a high height. MD = mental demand, PD = physical demand, TD = temporal demand, P = performance, E = effort, F = frustration. The error bar represents the mean \pm standard deviation. *: $p < 0.05$; **: $p < 0.01$; ***: $p < 0.001$.

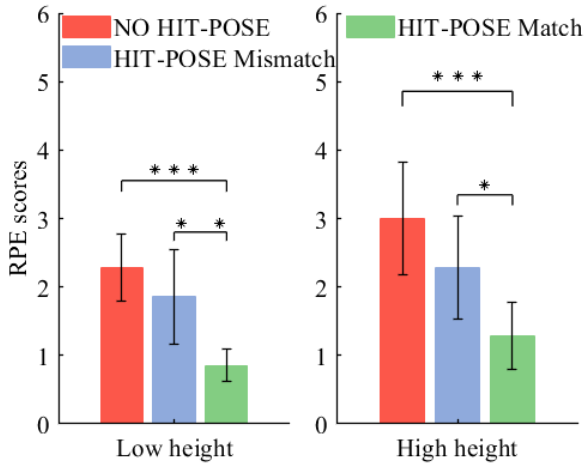


Fig. 15. RPE scores for each task among the three conditions from pairwise comparisons. The error bar represents the mean \pm standard deviation. *: $p < 0.05$; **: $p < 0.01$; ***: $p < 0.001$.

To ensure sufficient ROM while compactness, we extracted three parameters (ϕ , d_v , d_b) to design the shoulder structure, and two of them (d_v and d_b) can be adjusted without reconstructing the exoskeleton. A suitable set of parameters ($\phi=15^\circ$, $d_v=80\text{mm}$, $d_b=10\text{mm}$)

was selected through kinematic modeling and ROM simulations. Constrained but sufficient ROM was guaranteed in both sagittal and horizontal F/E for performing overhead work, as shown in Table V, while the structure with a relatively small volume ($22\text{cm} \times 48\text{cm} \times 15\text{cm}$) is designed to reduce the possibility of collision. Since volume information for other devices was not found, no comparison was made. However, our exoskeleton volume is visually more compact than its counterparts. The discrepancies between the ROM in simulations and experiments may be due to the omission of friction and contact forces in the simulations.

We had a trade-off for the shoulder movements, limiting the abduction/adduction movements of the shoulder, which are not the focus of overhead work. Through the coordination of sagittal and horizontal F/E joints, the exoskeleton can achieve abduction/adduction movements in the anterior space of the body, but there are limitations on movements in the posterior area of the body, such as extending the elbow diagonally backward and outward. This method meets the design requirements of the overhead work, and similar degree of freedom configuration strategies can be found on the ShoulderX [47] and Airframe [22]. As shown in Fig. 13, wearing the exoskeleton reduced hand workspace, likely due to a corresponding reduction in shoulder ROM.

B. Comparison of Adaptability with Existing Exoskeletons

Various overhead tasks and individuals usually have different PATAs and thus different optimal torque profiles [25], [26]. Consequently, the task and individual adaptability of the exoskeleton are crucial, which essentially involves adjustable PATA and peak torque. Existing exoskeletons have made considerable efforts in adjusting the assistive levels with different peak torque. Several exoskeletons employ a manual knob or an electrical component to adjust the assistive level, such as the Shoulder X [21] and H-PULSE [9], [13], other devices require to replace the spring or other parts affecting the spring length. However, existing exoskeletons can only adjust the amplitude of peak torque, thus just adapting to a specific task. Employing torque profiles with a fixed PATA to cope with all different tasks and individuals is not an energy-efficient way and limits the adaptability of the torque generator [26], [31]. For such exoskeletons, if we need to adjust the PATA, we can only change it by reconstructing the exoskeleton.

To enhance the task adaptability and personalized customization capability of the exoskeleton, we proposed a torque generator with an adjustable PATA. We utilized a set of parameters (α , β , r_1 , r_2 , r_3 , L_i) to guide the design of the torque generator, and investigated their impacts on torque profiles via geometric analysis and simulations. A subset of parameters (α , β , L_i) can be adjusted to reconfigure the exoskeleton, each controlling peak torque, PATA, and safety limit angle, respectively. Notably, β can be adjusted within a range of -30° to 30° , resulting in a range of PATA from 90° to 150° , which meets the requirements of various overhead tasks and individuals. The experimental results demonstrated that monitored muscular activations in HIT-POSE Match condition decreased the most compared to the NO HIT-POSE condition, thus validating the effectiveness of PATA. However, the exoskeleton provided an assistive torque of around 2 N-m when lowering the arm, which may cause discomfort to users. This is inevitable in our current design and also a limitation of the current architecture. Although this is not reflected in users' subjective evaluations, it may be attributed to the small sample size and individual sensitivity.

C. Effects of the Exoskeleton on Muscular Activations

For both tasks in HIT-POSE Match conditions, significantly reduced muscular activations were observed in agonist muscles (AD, MD, BB, PM, TR) and antagonist muscles (PD, LD) compared to NO HIT-POSE conditions. The exoskeleton provided support to the human shoulder, allowing agonist muscles to generate less force to achieve the same action, while also decreasing co-contraction of the antagonist muscles [13]. Similar results can be found in the ShoulderX [21], PAEXO [48], MATE [32], and H-VEX [26]. This phenomenon can be explained by the fact that there is a match between the PATA and the target task angle, resulting in increased assistive torque, with reductions consistent with the level of assistance [13], [49]. This also demonstrates the necessity of PATA for effective assistance. As reported by previous studies [50], [51], the reduced muscular activation implies lower force, resulting in decreased compressive force on the shoulder, and thus potentially reducing biomechanical stress on the shoulder girdle. Such positive effects suggest that long-term use of the exoskeleton has the potential to reduce the incidence of WMSDs, as reported by previous studies [17], [24].

Additionally, for screwing tasks in HIT-POSE Match conditions, the primary muscles (AD, MD, PD, BB, PM, and LD) significantly reduced their activations compared to HIT-POSE Mismatch conditions. The phenomenon is likely since a larger assistance was provided in HIT-POSE Match conditions, which provides evidence of our rational

design. Moreover, AD muscle in screwing at a low height did not exhibit a significant decrease between the two conditions. A previous study has shown that the activation reduction of AD muscle in high tasks is greater than that in low tasks [11], which may be a possible reason. Furthermore, the muscular activations of BB and TR muscles in screwing at a high height did not significantly change between the two conditions. In screwing at a high height, we observed that most participants involved more arm extension (except for lowering the arm), compared to screwing at a low height. The mechanical hysteresis of the spring contributes to larger assistance involving arm extension, which may preferentially transmit to BB muscle.

Notably, compared to NO HIT-POSE conditions, reductions in ES muscle were also expected for both tasks in HIT-POSE Match conditions. This behavior is consistent with the existing study [52]. This may be because the exoskeleton transmits forces to the waist through the device's back bar and waist belt. This result could indicate that HIT-POSE doesn't increase the risk of back WMSDs. An unexpected phenomenon is that the muscular activations in Fig. 14 were quite high. This could be attributed to our different normalization method, which does not affect the trend of EMG changes.

D. Effects of The Exoskeleton on Subjective Feedback

For both tasks in HIT-POSE Match conditions, the RPE displayed statistical significance from the other two conditions. Compared to NO HIT-POSE conditions, scores of the physical demand and effort items exhibited a significant reduction for both tasks in HIT-POSE Match conditions. Participants perceived the greatest assistance and thus exerted the lowest physical effort. This outcome is in line with the existing study [13]. In addition, for both tasks in HIT-POSE Match conditions, scores of the frustration item also exhibited a significant reduction with NO HIT-POSE conditions, which is consistent with the previous study [24]. Evidence may be available in a SUS question (9. I felt very confident using the system.) with a high average score (4.56 ± 0.53). We speculated that mental confidence bridges the frustration from the task, which may be related to a placebo effect. Meanwhile, the SUS score (79.7 ± 5.9) expressed good usability of the exoskeleton according to the empirical evaluation [53].

E. Limitations of The Study

While the experimental evaluations have shown positive effects, this study still has some limitations. Firstly, the PATA of the torque generator needs to be regulated manually. Consequently, one of our future works is to add a lightweight electrical element to adjust PATA automatically. Secondly, this experiment was conducted in a laboratory setting. Accordingly, the participants had no work experience. A field study and even the female participants would be considered in our further research. Thirdly, the long-term effect of the exoskeleton on users is not studied, which may exhibit different results. As the proposed prototype matures, we will investigate this issue, aiming to get a more complete and accurate assessment.

VI. CONCLUSION

In this study, we propose a passive occupational shoulder exoskeleton named HIT-POSE for overhead tasks, which enhances the adaptability of tasks and individuals while ensuring sufficient shoulder ROM. Firstly, we design an ergonomic shoulder structure by kinematic modeling and ROM simulations and verify through experiments. Secondly, we implement a torque generator with adjustable PATA through geometric analysis and simulations of torque profiles. Thirdly, we investigate the parameters' impacts on torque profiles to determine adjustable parameters to achieve various torque profiles

with different PATA without reconstructing the exoskeleton. Finally, we conduct experimental evaluations with aspects of objective and subjective within three conditions for two tasks, to validate the effectiveness of our proposed exoskeleton. Overall, the results have shown that HIT-POSE can decrease the physical load on users and has the potential to reduce the incidence of shoulder WMSDs.

In the future, we will strive to enhance the kinematic compliance of the exoskeleton to achieve a full ROM for the user. More realistic simulation algorithms of ROM will also be investigated to reduce the deviation between simulation and reality. In addition, a unique cam structure will be designed to further reduce the assistive torque at low elevation angles and improve the user acceptance and usability of the exoskeleton.

ACKNOWLEDGMENT

We gratefully acknowledge the participation of all individuals involved in this experiment. Their dedication and support were crucial to the completion of our research.

REFERENCES

- [1] A. Cieza *et al.*, "Global estimates of the need for rehabilitation based on the global burden of disease study 2019: a systematic analysis for the global burden of disease study 2019," *Lancet.*, vol. 396, no. 10267, pp. 2006–2017, Dec. 2020.
- [2] R. M. Enoka and J. Duchateau, "Muscle fatigue: what, why and how it influences muscle function," *J. Physiol.*, vol. 586, no. 1, pp. 11–23, Jan. 2008.
- [3] X. Wang *et al.*, "Work-related musculoskeletal disorders among construction workers in the united states from 1992 to 2014," *Occupat. Environ. Med.*, vol. 74, no. 5, pp. 374–380, Apr. 2017.
- [4] J. K. Sluiter *et al.*, "Criteria document for evaluating the work-relatedness of upper-extremity musculoskeletal disorders," *Scand. J. Work. Environ. Health.*, vol. 27, no. 1, pp. 1–102, 2001.
- [5] S. Ding *et al.*, "A lightweight shoulder exoskeleton with a series elastic actuator for assisting overhead work," *IEEE/ASME Trans. Mechatronics.*, vol. 29, no. 2, pp. 1030–1040, Apr. 2024.
- [6] K. Huysamen *et al.*, "Evaluation of a passive exoskeleton for static upper limb activities," *Appl. Ergonom.*, vol. 70, pp. 148–155, Jul. 2018.
- [7] D. Park *et al.*, "Shoulder-sidewinder (shoulder-side wearable industrial ergonomic robot): Design and evaluation of shoulder wearable robot with mechanisms to compensate for joint misalignment," *IEEE Trans. Robot.*, vol. 38, no. 3, pp. 1460–1471, Jun. 2022.
- [8] Y. M. Zhou *et al.*, "Kinematics-based control of an inflatable soft wearable robot for assisting the shoulder of industrial workers," *IEEE Robot. Autom. Lett.*, vol. 6, no. 2, pp. 2155–2162, Apr. 2021.
- [9] L. Grazi *et al.*, "Kinematics-based adaptive assistance of a semi-passive upper-limb exoskeleton for workers in static and dynamic tasks," *IEEE Robot. Autom. Lett.*, vol. 7, no. 4, pp. 8675–8682, Oct. 2022.
- [10] B. M. Otten *et al.*, "Evaluation of a novel active exoskeleton for tasks at or above head level," *IEEE Robot. Autom. Lett.*, vol. 3, no. 3, pp. 2408–2415, Jul. 2018.
- [11] J. Kim *et al.*, "A passive upper limb exoskeleton with tilted and offset shoulder joints for assisting overhead tasks," *IEEE/ASME Trans. Mechatronics.*, vol. 27, no. 6, pp. 4963–4973, Dec. 2022.
- [12] S. Crea *et al.*, "Occupational exoskeletons: A roadmap toward large-scale adoption. methodology and challenges of bringing exoskeletons to workplaces," *Wearable Technologies.*, vol. 2, p. e11, Sep. 2021.
- [13] L. Grazi *et al.*, "Design and experimental evaluation of a semi-passive upper-limb exoskeleton for workers with motorized tuning of assistance," *IEEE Trans. Neural. Syst. Rehabil. Eng.*, vol. 28, no. 10, pp. 2276–2285, Oct. 2020.
- [14] I. Pacifico *et al.*, "Exoskeletons for workers: A case series study in an enclosures production line," *Appl. Ergonom.*, vol. 101, p. 103679, May. 2022.
- [15] M. P. De Looze *et al.*, "Exoskeletons for industrial application and their potential effects on physical work load," *Ergonomics.*, vol. 59, no. 5, pp. 671–681, Aug. 2016.
- [16] S. De Bock *et al.*, "Passive shoulder exoskeletons: More effective in the lab than in the field?" *IEEE Trans. Neural. Syst. Rehabil. Eng.*, vol. 29, pp. 173–183, Dec. 2020.
- [17] S. DeBock *et al.*, "Passive shoulder exoskeleton support partially mitigates fatigue-induced effects in overhead work," *Appl. Ergonom.*, vol. 106, p. 103903, Jan. 2023.
- [18] S. Iranzo *et al.*, "Ergonomics assessment of passive upper-limb exoskeletons in an automotive assembly plant," *Appl. Ergonom.*, vol. 87, p. 103120, Sep. 2020.
- [19] M. Rossini *et al.*, "Design and evaluation of a passive cable-driven occupational shoulder exoskeleton," *IEEE Trans. Med. Robot. Bionics.*, vol. 3, no. 4, pp. 1020–1031, Nov. 2021.
- [20] M. B. Näf *et al.*, "Misalignment compensation for full human-exoskeleton kinematic compatibility: State of the art and evaluation," *Appl. Mech. Rev.*, vol. 70, no. 5, p. 050802, Sep. 2018.
- [21] J. P. Pinho and A. Forner-Cordero, "Shoulder muscle activity and perceived comfort of industry workers using a commercial upper limb exoskeleton for simulated tasks," *Appl. Ergonom.*, vol. 101, p. 103718, May. 2022.
- [22] T. C. McFarland *et al.*, "Level of exoskeleton support influences shoulder elevation, external rotation and forearm pronation during simulated work tasks in females," *Appl. Ergonom.*, vol. 98, p. 103591, Jan. 2022.
- [23] J. Hunt *et al.*, "A novel shoulder exoskeleton robot using parallel actuation and a passive slip interface," *J. Mech. Robot.*, vol. 9, no. 1, p. 011002, Feb. 2017.
- [24] S. De Bock *et al.*, "An occupational shoulder exoskeleton reduces muscle activity and fatigue during overhead work," *IEEE Trans. Biomed. Eng.*, vol. 69, no. 10, pp. 3008–3020, Oct. 2022.
- [25] P. Maurice *et al.*, "Objective and subjective effects of a passive exoskeleton on overhead work," *IEEE Trans. Neural. Syst. Rehabil. Eng.*, vol. 28, no. 1, pp. 152–164, Jan. 2019.
- [26] D. J. Hyun *et al.*, "A light-weight passive upper arm assistive exoskeleton based on multi-linkage spring-energy dissipation mechanism for overhead tasks," *Rob. Auton. Syst.*, vol. 122, p. 103309, Dec. 2019.
- [27] P. Yin *et al.*, "Effects of a passive upper extremity exoskeleton for overhead tasks," *J. Electromyogr. Kinesiol.*, vol. 55, p. 102478, Dec. 2020.
- [28] S. Kim *et al.*, "Assessing the influence of a passive, upper extremity exoskeletal vest for tasks requiring arm elevation: Part i—"expected" effects on discomfort, shoulder muscle activity, and work task performance," *Appl. Ergonom.*, vol. 70, pp. 315–322, Jul. 2018.
- [29] M. J. Jorgensen *et al.*, "Influence of different passive shoulder exoskeletons on shoulder and torso muscle activation during simulated horizontal and vertical aircraft squeeze riveting tasks," *Appl. Ergonom.*, vol. 104, p. 103822, Oct. 2022.
- [30] M. Jorgensen *et al.*, "The impact of passive shoulder exoskeletons during simulated aircraft manufacturing sealing tasks," *Int. J. Ind. Ergonom.*, vol. 91, p. 103337, Sep. 2022.
- [31] G. Vazzoler *et al.*, "Analysis and preliminary design of a passive upper limb exoskeleton," *IEEE Trans. Med. Robot. Bionics.*, vol. 4, no. 3, pp. 558–569, Aug. 2022.
- [32] I. Pacifico *et al.*, "An experimental evaluation of the proto-mate: a novel ergonomic upper-limb exoskeleton to reduce workers' physical strain," *IEEE Robot. Automat. Mag.*, vol. 27, no. 1, pp. 54–65, Mar. 2020.
- [33] J. R. Grieve and C. R. Dickerson, "Overhead work: Identification of evidence-based exposure guidelines," *Occupat. Ergon.*, vol. 8, no. 1, pp. 53–66, Sep. 2008.
- [34] J. Soucie *et al.*, "Range of motion measurements: reference values and a database for comparison studies," *Haemophilia.*, vol. 17, no. 3, pp. 500–507, Mar. 2011.
- [35] P. M. Ludewig *et al.*, "Motion of the shoulder complex during multi-planar humeral elevation," *J. Bone. Joint. Surg. Am.*, vol. 91, no. 2, pp. 378–389, Feb. 2009.
- [36] M. Stokdijk *et al.*, "The glenohumeral joint rotation centre in vivo," *J. Biomech.*, vol. 33, no. 12, pp. 1629–1636, Dec. 2000.
- [37] Z. Liu *et al.*, "Estimation for rotated center of shoulder in human upper limb dynamic motion measurement," *Journal of Tianjin University of Science and Technology*, vol. 22, no. 1, pp. 55–58, 2007. (in Chinese).
- [38] T. Nef *et al.*, "Armin iii—arm therapy exoskeleton with an ergonomic shoulder actuation," *Appl. Bionics. Biomech.*, vol. 6, no. 2, pp. 127–142, Jun. 2009.
- [39] H. J. Hermens *et al.*, "Development of recommendations for semg sensors and sensor placement procedures," *J. Electromyogr. Kinesiol.*, vol. 10, no. 5, pp. 361–374, Oct. 2000.
- [40] S. Song *et al.*, "Novice users' brain activity and biomechanics change after practicing walking with an ankle exoskeleton," *IEEE Trans. Neural. Syst. Rehabil. Eng.*, vol. 32, pp. 2522–2532, Jul. 2024.
- [41] G. Diamond-Ouellette *et al.*, "Exploring the influence of structured familiarization to an adjustable, passive load-bearing exoskeleton on oxygen consumption and lower limb muscle activation during walking,"

- IEEE Trans. Neural. Syst. Rehabil. Eng.*, vol. 32, pp. 2441–2449, Jun. 2024.
- [42] X. Peng and L. Stirling, “Examination of biofeedback to support the use of upper-extremity exoskeletons under proportional myoelectric control,” *IEEE Trans. Med. Robot. Bionics.*, vol. 6, no. 2, pp. 662–673, May. 2024.
- [43] S. G. Hart, “Nasa-task load index (nasa-tlx); 20 years later,” in *Proc. Hum. Factors Ergonom. Soc. Annu. Meeting.*, vol. 50, no. 9. Sage publications Sage CA: Los Angeles, CA, Oct. 2006, pp. 904–908.
- [44] G. Borg, “Psychophysical scaling with applications in physical work and the perception of exertion,” *Scandin. J. Work. Environ. Health.*, vol. 16, pp. 55–58, 1990.
- [45] J. Brooke, “Sus - a quick and dirty usability scale,” *Usability Eval. Ind.*, vol. 189, no. 194, pp. 4–7, 1996.
- [46] Z. Du *et al.*, “Development and experimental validation of a passive exoskeletal vest,” *IEEE Trans. Neural. Syst. Rehabil. Eng.*, vol. 30, pp. 1941–1950, Jul. 2022.
- [47] A. Ojelade *et al.*, “Three passive arm-support exoskeletons have inconsistent effects on muscle activity, posture, and perceived exertion during diverse simulated pseudo-static overhead nutrunning tasks,” *Appl. Ergonom.*, vol. 110, p. 104015, Jul. 2023.
- [48] P. Maurice *et al.*, “Evaluation of paexo, a novel passive exoskeleton for overhead work,” *Comput Methods Biomech Biomed Engin.*, vol. 22, no. sup1, pp. S448–S450, May. 2019.
- [49] L. Van Engelhoven *et al.*, “Experimental evaluation of a shoulder-support exoskeleton for overhead work: Influences of peak torque amplitude, task, and tool mass,” *IIEE Trans. Occupat. Ergon. Hum. Factors.*, vol. 7, no. 3-4, pp. 250–263, Jul. 2019.
- [50] S.-B. Lee and K.-N. An, “Dynamic glenohumeral stability provided by three heads of the deltoid muscle,” *Clin. Orthopaedics Rel. Res.*, vol. 400, pp. 40–47, Jul. 2002.
- [51] J. E. Labriola *et al.*, “Stability and instability of the glenohumeral joint: the role of shoulder muscles,” *J. Shoulder. Elbow. Surg.*, vol. 14, no. 1, pp. S32–S38, Feb. 2005.
- [52] L. S. Jakobsen *et al.*, “Biomechanical changes, acceptance, and usability of a passive shoulder exoskeleton in manual material handling. a field study,” *Appl. Ergonom.*, vol. 113, p. 104104, Nov. 2023.
- [53] A. Bangor *et al.*, “An empirical evaluation of the system usability scale,” *Int. J. Hum. Comput. Interact.*, vol. 24, no. 6, pp. 574–594, Jul. 2008.